BBA - Molecular Basis of Disease 1865 (2019) 1265–1272

Contents lists available at ScienceDirect

BBA - Molecular Basis of Disease

journal homepage: www.elsevier.com/locate/bbadis

Genetic, structural, and functional analysis of pathogenic variations causing methylmalonyl-CoA epimerase deficiency

Kathrin Heuberger[a,1], Henry J. Bailey[b,1], Patricie Burda[a], Apirat Chaikuad[b,2], Ewelina Krysztofinska[b,3], Terttu Suormala[a], Céline Bürer[a], Seraina Lutz[a], Brian Fowler[a], D. Sean Froese[a], Wyatt W. Yue[b,*], Matthias R. Baumgartner[a,*]

[a] Division of Metabolism and Children's Research Center, University Children's Hospital, Steinwiesstrasse 75, CH-8032 Zurich, Switzerland
[b] Structural Genomics Consortium, Nuffield Department of Medicine, University of Oxford, Old Road Campus Research Build, Roosevelt Dr, Oxford, OX3 7DQ, UK

ARTICLE INFO

Keywords:
Methylmalonic aciduria
Rare disease
Methylmalonyl-CoA epimerase
Crystal structure
Missense variant
Protein misfolding

ABSTRACT

Human methylmalonyl-CoA epimerase (*MCEE*) catalyzes the interconversion of D-methylmalonyl-CoA and L-methylmalonyl-CoA in propionate catabolism. Autosomal recessive pathogenic variations in *MCEE* reportedly cause methylmalonic aciduria (MMAuria) in eleven patients. We investigated a cohort of 150 individuals suffering from MMAuria of unknown origin, identifying ten new patients with pathogenic variations in *MCEE*. Nine patients were homozygous for the known nonsense variation p.Arg47* (c.139C > T), and one for the novel missense variation p.Ile53Arg (c.158T > G). To understand better the molecular basis of MCEE deficiency, we mapped p.Ile53Arg, and two previously described pathogenic variations p.Lys60Gln and p.Arg143Cys, onto our 1.8 Å structure of wild-type (wt) human MCEE. This revealed potential dimeric assembly disruption by p.Ile53Arg, but no clear defects from p.Lys60Gln or p.Arg143Cys. We solved the structure of MCEE-Arg143Cys to 1.9 Å and found significant disruption of two important loop structures, potentially impacting surface features as well as the active-site pocket. Functional analysis of MCEE-Ile53Arg expressed in a bacterial recombinant system as well as patient-derived fibroblasts revealed nearly undetectable soluble protein levels, defective globular protein behavior, and using a newly developed assay, lack of enzymatic activity - consistent with misfolded protein. By contrast, soluble protein levels, unfolding characteristics and activity of MCEE-Lys60Gln were comparable to wt, leaving unclear how this variation may cause disease. MCEE-Arg143Cys was detectable at comparable levels to wt MCEE, but had slightly altered unfolding kinetics and greatly reduced activity. These studies reveal ten new patients with MCEE deficiency and rationalize misfolding and loss of activity as molecular defects in MCEE-type MMAuria.

1. Introduction

Propionyl-CoA is the common degradation product from branched-chain amino acids, odd-chain fatty acids, and the side chain of cholesterol. The propionate catabolic pathway serves to funnel propionyl-CoA into the tricarboxylic acid (TCA) cycle for use as cellular energy sources through oxidative phosphorylation. Located at the centre of this pathway, methylmalonyl CoA epimerase (MCEE) catalyzes the epimerization of D-methylmalonyl-CoA, generated from propionyl-CoA by propionyl-CoA carboxylase (PCC), to form L-methylmalonyl-CoA, subsequently converted into succinyl-CoA by methylmalonyl-CoA mutase (MUT) for entry into the TCA cycle.

Isolated methylmalonic aciduria (MMAuria), an inborn error of organic acid metabolism, is typically caused by deficiency of MUT or by a defect in the transport or processing of its organometallic cofactor, adenosylcobalamin. However, pathogenic variations in the human *MCEE* gene (OMIM #251120) have been identified in eleven cases of atypical MMAuria [1–6]. For two patients, coincidental variations in the *SPR* gene causing sepiapterin reductase deficiency sufficiently explained their clinical symptoms [2,4], while two others have been described as asymptomatic [3], leaving the clinical importance of MCEE deficiency in doubt. The majority of patients with MCEE deficiency

* Corresponding authors.
E-mail addresses: wyatt.yue@sgc.ox.ac.uk (W.W. Yue), Matthias.Baumgartner@kispi.uzh.ch (M.R. Baumgartner).
[1] Equal contribution.
[2] Present address: Institute of Pharmaceutical Chemistry & Structural Genomics Consortium, BMLS, Goethe-University Frankfurt, 60438 Frankfurt, Germany.
[3] Present address: Astex Pharmaceuticals, 436 Cambridge Science Park, Milton Road, Cambridge, CB4 0QA, UK.

https://doi.org/10.1016/j.bbadis.2019.01.021
Received 15 November 2018; Received in revised form 16 January 2019; Accepted 18 January 2019
Available online 22 January 2019
0925-4439/ © 2019 The Authors. Published by Elsevier B.V. This is an open access article under the CC BY license (http://creativecommons.org/licenses/BY/4.0/).

(seven including those with sepiapterin reductase deficiency) are homozygous for the stop-gain nonsense variation c.139C > T (p.Arg47*) [1–6]; the missense changes p.Lys60Gln and p.Arg143Cys [3] and a splice altering variation (c.379-644A > G) [5] have also been identified, but the functional relevance of these remains unclear.

In the human genome, MCEE is one of six proteins belonging to the vicinal oxygen chelate (VOC) superfamily, which include also glyoxalase I (*GLO1* gene, GLOD1 protein), 4-hydroxyphenylpyruvic acid dioxygenase (*HPD*, GLOD3), 4-hydroxyphenylpyruvic acid dioxygenase-like (*HPDL*, GLOXD1), and glyoxalase domain-containing 4 (*GLOD4*) and 5 (*GLOD5*). VOC members are metalloenzymes highly divergent in sequence and biological functions, but universally share the use of the βαβββ structural motif (also known as the glyoxylase fold) to build a divalent metal-containing active site [7,8]. VOC enzymes catalyze a range of chemical reactions including isomerization, epimerization, oxidative C—C bond cleavage and nucleophilic substitution [9]. The active-site divalent metal is used to bind the reaction substrate, intermediates or transition states in a bidentate fashion [8]. To date, only structures from bacterial MCEE orthologues (*Propionibacterium shermanii* and *Thermoanaerobacter tengcongensis*) have been reported [10,11].

In this article, we conducted an in depth investigation of MCEE deficiency at the gene and protein levels. From a cohort of 150 patients with MMAuria of unknown etiology, we identified ten new patients with pathogenic variations on the *MCEE* gene including a novel missense change. We determined the crystal structure of human MCEE of the wild-type as well as p.Arg143Cys variant proteins. We further characterized protein expression and enzyme activity for the three known MCEE missense changes associated with disease. Our study provides a molecular explanation for the biochemical defects associated with pathogenic missense variations.

2. Materials and methods

2.1. Reagents

Unless otherwise noted, all compounds were obtained from Sigma-Aldrich (Buchs SG, Switzerland) and were reagent grade or better.

2.2. Purification, crystallization and structure determination of hMCEE

Human (h) MCEE was cloned, expressed and purified as previously described [12]. Briefly, wt and variant proteins were expressed in *Escherichia coli* BL21(DE3)R3-Rosetta cells from 3 to 6 l of Terrific Broth culture. Cell pellets were lysed by high pressure homogenizer and centrifuged at 35,000 ×*g*. The clarified cell extract was incubated with 2.5 ml of Ni-NTA resin pre-equilibrated with lysis buffer (50 mM HEPES pH 7.5, 500 mM NaCl, 10 mM Imidazole, 5% Glycerol, 0.5 mM TCEP). The column was washed with 100 ml Binding Buffer (50 mM HEPES pH 7.5, 500 mM NaCl, 5% glycerol, 10 mM Imidazole, 0.5 mM TCEP), 50 ml Wash Buffer (50 mM HEPES pH 7.5, 500 mM NaCl, 5% glycerol, 40 mM Imidazole, 0.5 mM TCEP) and eluted with 15 ml of Elution Buffer (50 mM HEPES pH 7.5, 500 mM NaCl, 5% glycerol, 250 mM Imidazole, 0.5 mM TCEP). The eluant fractions were concentrated to 5 ml and applied to a Superdex 200 16/60 column pre-equilibrated in GF Buffer (10 mM HEPES pH 7.5, 500 mM NaCl, 0.5 mM TCEP, 5% glycerol). Eluted protein fractions were incubated with 1:20 mol:mol TEV protease overnight at 4 °C. The next day sample was passed through 0.5 ml Ni-NTA pre-equilibrated with GF Buffer and washed 1 ml of GF Buffer. Flow-through and wash were pooled and concentrated to 10–15 mg/ml.

Crystals of $hMCEE_{WT}$ were grown by vapour diffusion in sitting drop at 20 °C. A sitting drop consisting of 75 nl protein and 75 nl well solution was equilibrated against well solution containing 30% (v/v) low molecular weight PEG smear [13] and 0.1 M Tris pH 8.5. Crystals were mounted in the presence of 25% (v/v) ethylene glycol and flash-cooled in liquid nitrogen. Crystals of $hMCEE_{R143C}$ were grown by vapour diffusion in sitting drop at 20 °C. A sitting drop consisting of 50 nl protein and 100 nl well solution was equilibrated against well solution containing 20% PEG4000, 10% 2-propanol and 0.1 M HEPES pH 7.5. Crystals were mounted in the presence of 25% (*v*/v) ethylene glycol and flash-cooled in liquid nitrogen. Crystallization and diffraction data are given in Table 2. The structure of $hMCEE_{WT}$ was solved by molecular replacement using PHASER [14], with *P. shermanii* MCEE structure (PDB 1JC5) as search model. The structure of $hMCEE_{R143C}$ was solved by molecular replacement with $hMCEE_{WT}$ as search model. Iterative cycles of refinement and manual model building were performed using COOT [15], REFMAC5 [16] and phenix.refine [17].

2.3. Size exclusion chromatography

Size exclusion chromatography was performed as described in [18].

2.4. Nano-differential scanning fluorimetry

Melting curves for the wt protein and mutants were obtained via detection of changes in light scattering using the Prometheus NT.48. Protein concentration was kept at 100 μM in 50 mM HEPES pH 7.5, 500 mM NaCl, 0.5 mM TCEP, 5% glycerol and a melt gradient of 1° per minute 20 °C to 95 °C was used.

2.5. Patient characterization (genotyping, propionate incorporation)

Skin fibroblasts were taken from patients with biochemical and clinical evidence of methylmalonic aciduria, referred to our institution for diagnostic purposes. The study has been approved by the ethics commission of the Canton of Zurich, Switzerland (application no. 2014-0211). Genomic DNA and RNA extraction, as well as sequencing and propionate incorporation were performed as previously described [18]. The nomenclature of the variation is based on the cDNA sequence NM_032601.3. Nucleotide numbering uses +1 as the A of the ATG translation initiation codon in the reference sequence, with the initiation codon as codon 1.

2.6. Transfection, immunoblotting and enzymatic assay

A DNA fragment encompassing the entire coding sequence of wild-type MCEE was cloned into pcDNA3-CT10HF-LIC using LIC cloning. The sequence was as given by NM_032601.3, except for c.311 T > G (p.Leu104Arg), whereby c.311G is the more common allele, [19]. Site-directed mutagenesis was carried out on this construct using the QuikChange site-directed mutagenesis kit (Stratagene, La Jolla, CA) as described in the manufacturer's instructions, using forward and reverse primers (Microsynth, Balgach, Switzerland) and confirmed by Sanger sequencing. Control (BJ, CRL-2522, ATCC) or patient (carrying homozygous MCEE c.139C > T, p.Arg47*) fibroblasts were transiently transfected with 10 μg wild-type or mutant MCEE constructs, with or without 10 μg MUT in pTracer [20] for the enzymatic assay, using electroporation [21]. Cells were grown in Dulbecco's Modified Eagle Medium (Gibco) supplemented with 10% fetal bovine serum (Gibco) and antibiotics (GE Healthcare), as previously described [22] and harvested by trypsinization 48 h after electroporation, washed twice with HBSS (Gibco) and either frozen at −20 °C or processed directly.

Western Blot analysis was performed on fresh or frozen cell pellets essentially as described in [20], with the exception that monoclonal anti-flagM2 (1:4,000; Sigma–Aldrich) and anti-β-Actin (at 1:5,000; Sigma–Aldrich) were used.

For the enzymatic assay, fresh or frozen cell pellet was lysed in buffer including 12 mM Tris-HCl, pH 8.0 and 1 mM DTT with sonication twice at amplitude 1.5 for 15 s using the microprobe of an XL-2000 sonicator (Microson, Qsonica Newtown, CT). Following lysis, protein concentration was determined by the Lowry method. The incubation

mixture contained 300–500 µg cell protein, reaction buffer (100 mM Tris-HCl, pH 8.0; 6 mM $MgCl_2$; 3.15 mM ATP; 100 mM KCl; 3 mM DTT), 1 mM propionyl-CoA mix (1 mM propionyl-CoA and 7 µM [^{14}C]-propionyl-CoA at 55 mCi/mmol, Anawa, Switzerland) and 50 uM adenosylcobalamin and reaction time was 60 min at 37 °C. The reaction was stopped by adding 0.5 M KOH, samples were then re-incubated for 15 min at 37 °C to hydrolyze CoA derivatives, neutralized by adding 0.5 N perchloric acid (Merck), and spiked with 0.05% succinic acid, 0.018% methylmalonic acid and 0.018% propionic acid in order to visualize peaks during HPLC separation. Samples were centrifuged to remove precipitate, and supernatant was injected into an Aminex HPX-87H Ion Exclusion column (300 × 7.8 mm2; H-form, 9 µm, Bio-Rad), and organic acids separated by elution with 0.5 mM H_2SO_4 at 30 °C using a flow rate of 0.4 ml/min. Retention times were 13–15 min for methylmalonic acid, 17–19 min for succinic acid, and 26–28 min for propionic acid (Supplemental Fig. S5 and 6), visualized at 210 nm using a UV detector. Fractions covering the methylmalonic acid and succinic acid peaks were collected and [^{14}C]-methylmalonic acid and [^{14}C]-succinic acid quantified in a Tri-Carb C1 900TR scintillation spectrometer (PerkinElmer,Waltham, MA, USA) with OptiphaseHiSafe 2 counting cocktail (PerkinElmer).

3. Results & discussion

3.1. Identification of ten new MCEE patients with methylmalonic aciduria

Thus far, 11 cases of MMAuria have been identified due to pathogenic variations in the *MCEE* gene [1–6]. We screened fibroblast cell lines taken from 150 patients with mild but clear MMAuria who could not be assigned to a cobalamin class of defect. From this cohort, we identified ten patients from nine families with pathogenic variations in *MCEE* (Table 1). Nine patients were homozygous for the c.139C > T (p.Arg47*) nonsense variation, which has been previously described. This remains by far the most common pathogenic variation identified in MCEE deficiency, with 16 out of 21 patients homozygous for this allele. One patient in our cohort was homozygous for c.158 T > G (p.Ile53Arg), a novel missense variation that is not found in the ExAC database (> 120,000 alleles) [19]. We did not observe either c.178A < C (p.Lys60Gln), previously found in one patient in the homozygous state, or c.427C > T (p.Arg143Cys), previously found in two patients in the heterozygous state without an apparent second disease causing variation [3].

In our cohort, disease onset ranged from 1 month old to 2.5 years of age, while from two patients we had no information. Clinical symptoms were variable but usually mild, and no patient was responsive to vitamin B_{12} treatment. At least three patients presented following an intercurrent illness, while three presented with metabolic acidosis and/or hypoglycemia. In addition, elevated levels of other metabolites typical for a block in the propionate degradation pathway, such as 2-methylcitrate, propionylcarnitine and 3-hydroxypropionate, were documented in most patients. Investigation in patient fibroblasts revealed mildly decreased propionate incorporation (Table 1), which did not increase upon addition of hydroxocobalamin.

3.2. Structural features of human MCEE

We performed structural biology studies to establish the molecular basis of disease-causing variations on the human MCEE protein (hMCEE). As a first step, we determined the crystal structure of wild-type (wt) protein ($hMCEE_{WT}$) to 1.8 Å resolution (Table 2), as part of a wider effort that also generated crystal structures of three other human VOCs, namely hHPD (PDB: 3ISQ), hGLOD4 (PDB 3ZI1) and hGLOD5 (PDB 3ZW5). Most VOC members are structurally made up of four glyoxylase (GLOD) motifs of βαββ topology. As exemplified in Supplemental Fig. S1, the human VOCs display versatility in the way that four GLOD motifs are assembled, at the gene or protein level, to give

Table 1
List of ten newly identified MCEE patients with relevant genetic, biochemical and clinical data.

Patient no.	Age at onset	Variation[a]	Clinical presentation, laboratory data	Urinary MMA	Propionate incorporation[b] nmol/16 h/mg	
		Homozygous for all patients		mmol/mol creat.	−OHCbl	+OHCbl
				Ref. 0.3–1.1	Ref. 3.5–24.4	Ref. 4.3–28.9
1	4 mo	c.139C > T; p. Arg47*	Cardiomyopathy. Sibling with similar biochemical profile but no symptoms	441	1.9 (1.8–2.0)	1.9 (1.8–2.1)
2	2 yr	c.139C > T; p. Arg47*	Severe metabolic acidosis and hypoglycemia following gastroenteritis, elevated propionyl-carnitine; 3-OH propionate & methyl-citrate in urine	458	1.9 (1.8–2.1)	2.0 (1.8–2.1)
3	2.5 yr	c.139C > T; p. Arg47*	Severe metabolic acidosis, elevated propionyl-carnitine; 3-OH propionate & methyl-citrate	Elevated	1.4 (1.2–1.5)	1.4 (1.2–1.6)
4	1.5 yr	c.139C > T; p. Arg47*	Severe metabolic acidosis and hypoglycemia following intercurrent illness	594	2.0 (1.8–2.3)	1.9 (1.5–2.4)
5[c]	–	c.139C > T; p. Arg47*	No data; enzyme assays performed at 3 years of age	Elevated	3.0 (2.9–3.0)	3.0 (2.9–3.4)
6[c]	–	c.139C > T; p. Arg47*	No data; enzyme assays performed at 7 years of age	Elevated	2.7 (2.6–3.0)	2.7 (2.4–2.9)
7	2 yr	c.139C > T; p. Arg47*	Slow motor development, hypotonia (inability to walk independently), spasticity of legs, eczema, episode of vomiting and diarrhea	143	2.5 (2.2–2.8)	2.5 (2.3–2.7)
8	1 mo	c.139C > T; p. Arg47*	Sepsis, psychomotor retardation, seizures, elevated C3-acylcarnitine, methyl-citrate in urine	Elevated	2.0 (1.8–2.1)	2.0 (1.9–2.2)
9	6 mo	c.158 T > G; p.Ile53Arg	Seizures and hypoglycemia following viral infection, elevated proionyl-carnitine; methyl-citrate in urine; then normal development	143–184	3.0 (2.9–3.2)	3.0 (2.9–3.1)
10	< 1 yr	c.139C > T; p.Arg47*	Ketoacidosis	Elevated	2.4 (2.4–2.3)	2.4 (2.4–2.4)

[a] According to NM_032601 and NP_1159990. Nucleotide numbering uses + 1 as the A of the ATG translation initiation codon in the reference sequence, with the initiation codon as codon 1.
[b] [^{14}C]propionate incorporation: fibroblasts were grown for 3 days without (−) and with (+) 10 mg of hydroxocobalamin (OH-Cbl)/ml medium. Values for patient cells represent mean and range (in brackets) from 3 replicate experiments. For controls (WT) the range of 33 individual fibroblast cell lines is given.
[c] Patient 5 and patient 6 are siblings.

Table 2
Data collection and refinement statistics for the crystal structures. Data from highest resolution shell shown in parenthesis.

Dataset	$hMCEE_{WT}$	$hMCEE_{R143C}$
Beamline	Diamond beamline I02	Diamond beamline I04
Wavelength (Å)	0.9763	0.9795
Unit cell parameters (a,b,c)	53.12 Å, 66.69 Å, 76.98 Å	53.16 Å, 66.99 Å, 77.13 Å
(α, β, γ)	90.0°, 90.1°, 90.0°	90.00°, 90.02°, 90.00°
Space group	P 1 21 1	P 1 21 1
Resolution range (Å)	36.58–1.80	77.13–1.92[a]
Observed/Unique reflections	49,519	19,630
Rsym (%)	0.076 (0.56)	0.13 (0.92)
I/sig(I)	1.98	7.2 (1.2)
Completeness (%)	99.2 (99.7)	88.9 (55.8)
Multiplicity	3.6 (3.6)	3.3 (2.7)
R_{cryst} (%)	0.19	0.23
R_{free} (%)	0.238	0.28
Wilson *B* factor (Å^2)	23.7	25
Average total *B* factor (Å^2)	27.59	35.6
R.m.s.d. bond length (Å^2)	0.67	0.003
R.m.s.d. bond angle (°)	0.69	0.588
Missing residues	1–44	1–44
Clashscore	6	4.29
Ramachadran favoured (%)	97	99
Ramachandran disallowed (%)	1	0
Rotamer outliers (%)	0	0

[a] Anisotropic data truncated in staraniso using local I/sigI cut off at 1.2 results in the inclusion of data to 1.9 Å with outer-shell ellipsoidal completeness at 58.8% and spherical completeness at 10%.

rise to a minimal functional unit harbouring two metal-binding active sites.

In the case of hMCEE, two βαβββ motifs pack side-by-side to form an 8-stranded sheet that completes the active site for one protomer (Fig. 1A). Crystallographic (Supplemental Fig. S1) and solution data (Supplemental Fig. S2) show that hMCEE is dimeric, in agreement with bacterial orthologs [10,11]. The VOC members are so called because a divalent metal per active site can bind the substrate, intermediates or transition states in a bidentate fashion [8]. The divalent metal ion in hMCEE, observed as cobalt in our structure, is coordinated by three residues strictly conserved among VOCs: His50 (strand β1), His122 (strand β5), and Glu172 (strand β8) (Fig. 1B).

3.3. Structural mapping of missense variations

Both the reported p.Arg143Cys and newly identified p.Ile53Arg missense changes are predicted by SIFT (Damaging, score: 0.00 & 0.01) and PolyPhen2 (Probably damaging, score: 0.989 & 1.00) to be deleterious. By contrast, the other previously reported p.Lys60Gln variation was predicted to be not deleterious (SIFT: 0.12 tolerated, PolyPhen2: 0.04 benign). The most common pathogenic variation of MCEE, c.139C > T, causes truncation of the protein at p.Arg47*, within the first β-sheet (Supplemental Fig. S3). Loss of almost the entire protein is therefore the likely cause of enzymatic dysfunction due to this variation, assuming there is residual mRNA following nonsense-mediated decay.

By contrast, the molecular dysfunction due to the missense variations is less clear (Fig. 1C). In our hMCEE structure, Ile53 is located at the dimeric interface, making hydrophobic contacts with Gly168 and Val169 from the loop region connecting strands β7 and β8 ($loop_{β7\text{-}β8}$) of the other subunit in the dimer, (Fig. 1D). The amino acid (aa) position of Ile53 is highly conserved among MCEE orthologues (85% occupied by Ile, n = 150). An Ile-to-Arg at this position likely interferes with proper dimeric assembly, and is predicted by FoldX [23] to have severely reduced stability (ΔΔG 9.53 kcal/mol). By contrast, Lys60 and Arg143 occupy amino acid positions that are more variable. Position 60 is only occupied by lysine in 15% of MCEE homologs while position 143 is 60% occupied by arginine. Both residues are surface exposed and not directly involved in the dimeric interface and active-sites of both subunits (Fig. 1D), consistent with a FoldX prediction of no effect for p.Lys60Gln (ΔΔG 0.3 kcal/mol), and moderately reduced stability for p.Arg143Cys (ΔΔG 2.26 kcal/mol).

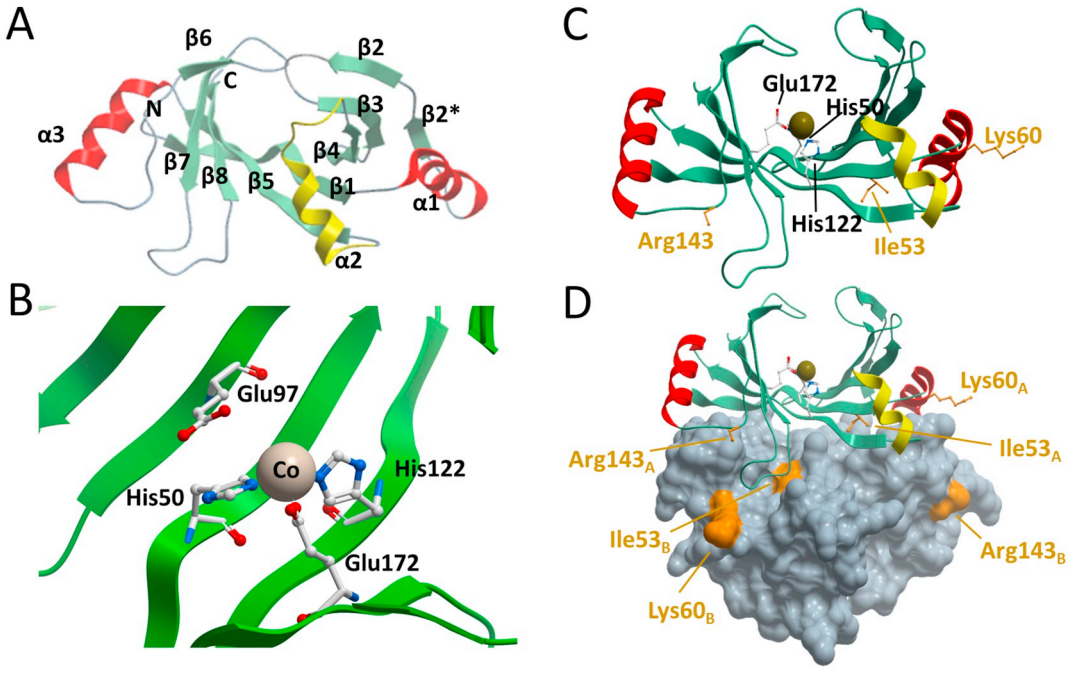

Fig. 1. Structure of hMCEE (PDB ID:3RMU). A. Monomeric structure coloured by secondary structure, whereby β-strands are green, α-helices that are part of the GLOD motif are red, and regions that connect GLOD motifs are yellow. B. Active-site architecture showing the divalent metal and metal coordinating residues. Pink sphere: cobalt. C. On the hMCEE monomer, residues that are mutated in disease are labeled in orange, active-site residues are labeled in black. D. hMCEE physiological dimer with the second subunit represented as grey space fill. Missense changes are labeled in orange and designated as belonging to chain (monomer) A or B.

3.4. Structure of human MCEE p.Arg143Cys variant

We determined the crystal structure of the p.Arg143Cys variant protein ($hMCEE_{R143C}$) to 1.9 Å resolution (Table 2), to directly inspect the atomic environment of the substitution (Fig. 4). While $hMCEE_{R143C}$ superimposes well overall with $hMCEE_{WT}$ (Cα-RMSD 0.278 Å), significant main-chain displacement was clearly observed in the loop region connecting helix α3 and β6 ($loop_{α3-β6}$) that harbours the site of change at aa 143, as well as the nearby $loop_{β7-β8}$ (Fig. 2, inset). These loop regions connect several β-strands that make up the protomer active site. In the $hMCEE_{R143C}$ structure, the substituted Cys143 residue generated more mobility and disorder within the $loop_{α3-β6}$. As a result, the main-chain atoms of aa 142–146 are displaced by ~2.5–4.7 Å compared to $hMCEE_{WT}$. The increased mobility in $loop_{α3-β6}$ impacts on the nearby $loop_{β7-β8}$ that packs against it, resulting in 2.0–4.8 Å main-chain displacement at the first half of $loop_{β7-β8}$ (aa 164–167). The second half of $loop_{β7–β8}$, involved in the aforementioned dimeric interface, was not affected by any displacement. Together, these local structural changes have the potential to impact on the surface features of the homodimer, as well as the active site pocket.

3.5. Characterization of missense variations in recombinant and patient cells

To validate our structural interpretation, we performed expression studies in *E. coli* and human cells. When expressed in *E. coli* (Fig. 3A), hMCEE wt, p.Lys60Gln and p.Arg143Cys proteins were highly soluble, while the p.Ile53Arg variant showed a massive decrease in protein solubility, consistent with a poorly folded protein. All wt and variant hMCEE molecules eluted at similar volumes by size exclusion chromatography (Supplemental Fig. S4). Thermal unfolding (Fig. 3B) of purified hMCEE p.Ile53Arg by nano-differential scanning fluorimetry revealed a melting curve of multiple transitions, indicative of heterogenous protein states. By contrast, purified wt and p.Lys60Gln proteins showed globular protein behaviour reflected by a cooperative sigmoidal melting pattern, indicating a single unfolding/folding transition. p.Arg143Cys also behaved similarly to wt and p.Lys60Gln, however late stage unfolding/folding intermediates deviate from sigmoidal melting. Together our data indicate reduced thermostability for the p.Ile53Arg variant protein and a potential slight alteration in that of p.Arg143Cys.

These results were validated by over-expression of hMCEE in patient fibroblasts homozygous for the *MCEE* null variant (c.139C > T;

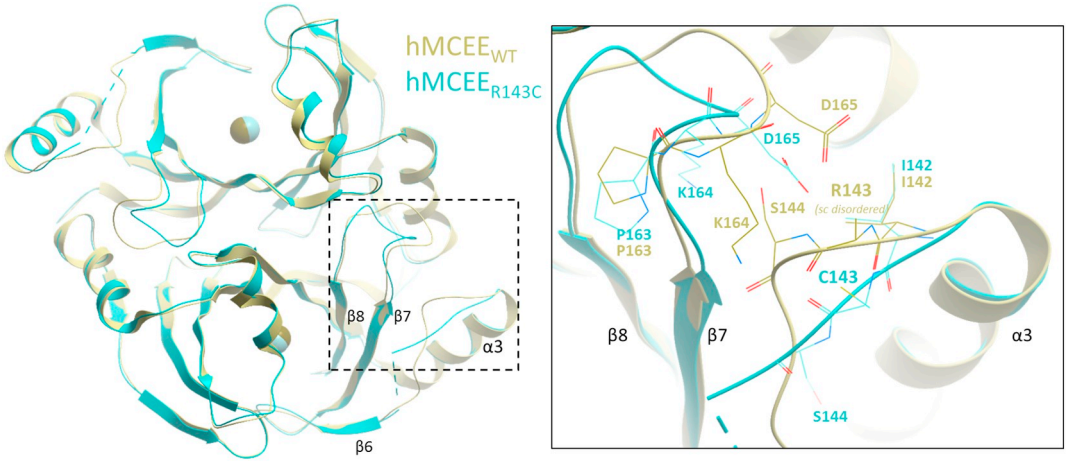

Fig. 2. Structure of hMCEE p.Arg143Cys variant (PDB ID:6QH4). Structural superposition of hMCEE homodimer from $hMCEE_{WT}$ (yellow) and $hMCEE_{R143}$ (cyan) proteins. *Inset*. Magnified view of the local atomic environment surrounding the Arg143/Cys143 site, where amino acid side-chains are shown as thin lines.

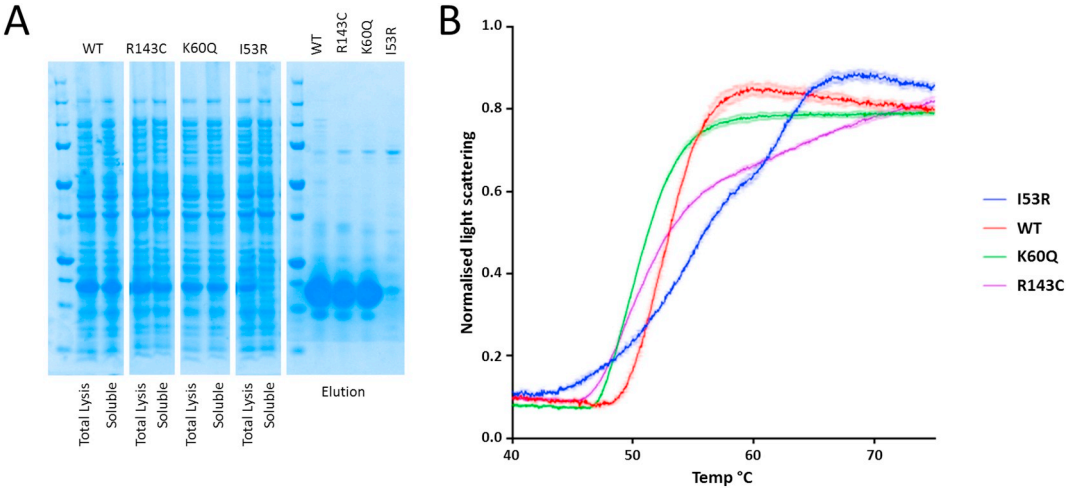

Fig. 3. Characterization of recombinant hMCEE wt and variant proteins. A. SDS-PAGE analysis of hMCEE protein expression (from cell lysate: Total Lysis; and centrifuged supernatant fractions: Soluble) and solubility (from eluant fractions of affinity purification); B. nanoDSF melting curve plot of normalized light scattering intensity against temperature.

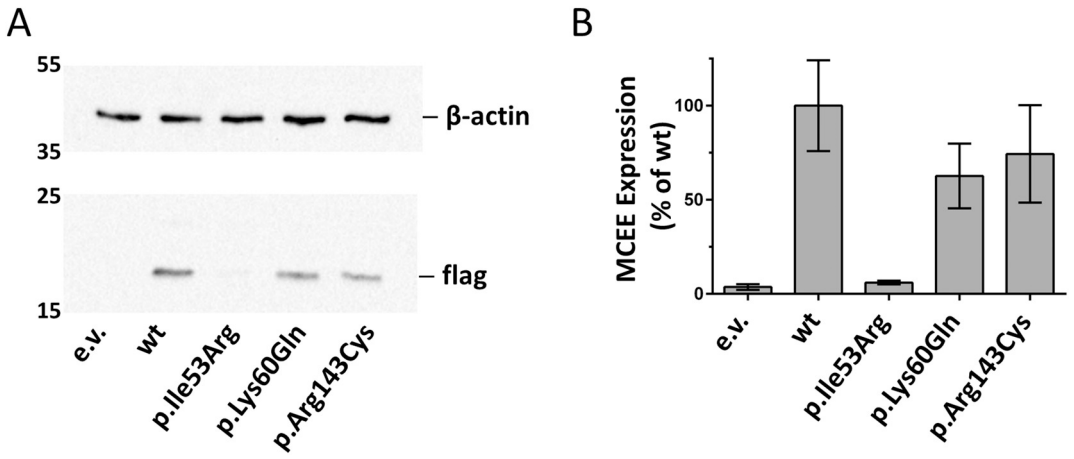

Fig. 4. Over-expression of hMCEE-flag in human fibroblasts. A. Representative Western blots depicting detection of wild-type (wt) or mutant hMCEE-flag following over-expression in patient fibroblasts deficient for MCEE enzyme. Vector without insert was used as a control (e.v.). Loading was controlled by detection of endogenous β-actin. Numbers on the left correspond to molecular weights (kDa). Approximate expected molecular weights, hMCEE-flag: 18 kDa; β-actin: 42 kDa. B. Bar-graph depicting mean and standard deviation of Western blot results performed in 3 independent experiments.

p.Arg47*). For this experiment, flag-tagged wt and mutant hMCEE proteins were over-expressed with visualization of the flag-tag by Western blot analysis (Fig. 4A). Expression of each construct performed at least 3 times revealed wt protein to be well expressed, while hMCEE containing p.Lys60Gln and p.Arg143Cys were detectable at only slightly lower levels (63 ± 17% and 74 ± 26% of wt, respectively) (Fig. 4B). However, hMCEE containing p.Ile53Arg had very low levels of detectable protein (6 ± 1% of wt), similar to empty vector (4 ± 2% of wt) (Fig. 4B). Thus, consistent with recombinant studies, it appears that p.Ile53Arg causes an inability to fold correctly.

3.6. Biochemical characterization of missense variations

We developed a radioactive HPLC-based assay to assess MCEE activity of wt and variants. This assay follows the production and separation of [^{14}C]-methylmalonic acid and [^{14}C]-succinic acid from [^{14}C]-propionic acid following addition of [^{14}C]-propionyl-CoA to fibroblast cell lysates, as depicted in Fig. 5A. Using UV detection, we were able to detect separated propionic acid, methylmalonic acid and succinic acid following HPLC analysis (Supplemental Fig. S5). In cell lysates from control fibroblasts, we identified high levels of [^{14}C]-methylmalonic acid but only very little [^{14}C]-succinic acid (Fig. 5B;

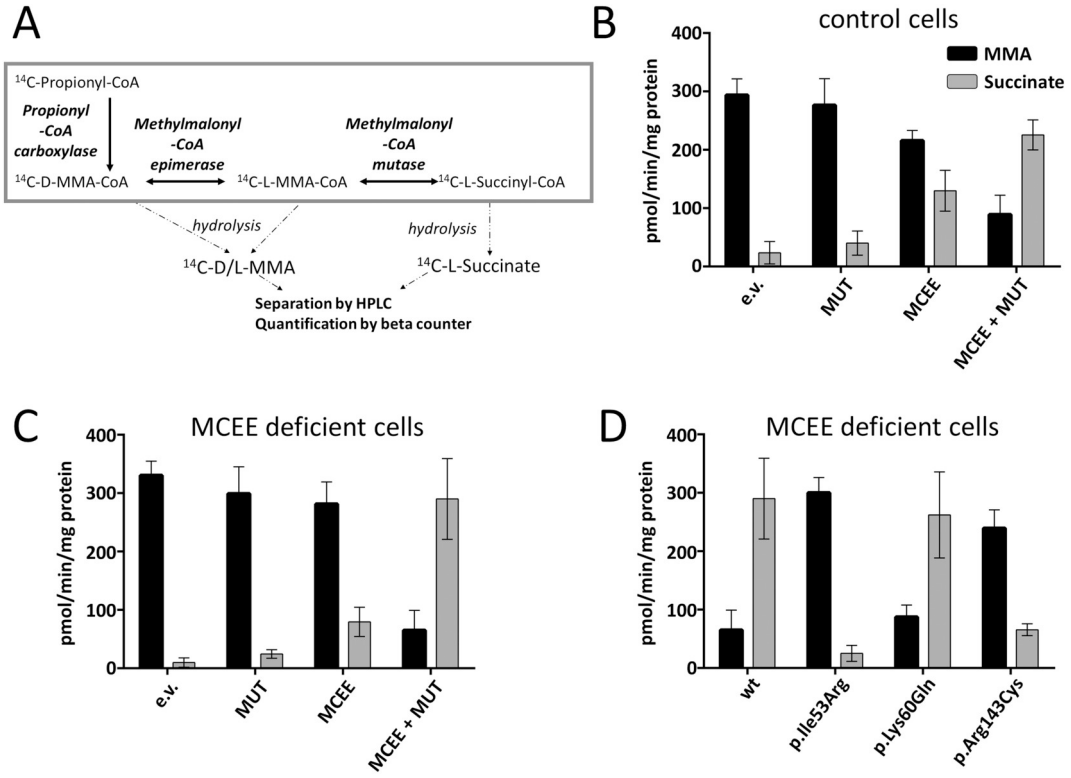

Fig. 5. Biochemical analysis of hMCEE disease associated variations. A. Schematic depiction of the cellular pathway leading from propionyl-CoA to succinyl-CoA and the enzymes involved in this process. B and C. Bar-graph showing the amount of methylmalonic acid (MMA) and succinate following over-expression of empty vector (e.v.), methylmalonyl-CoA mutase (MUT) alone, MCEE alone, or both MCEE and MUT in control fibroblasts (B) and patient fibroblasts deficient in MCEE (C). D. Bar graph depicting production of MMA and succinate following over-expression of wild-type (wt) and mutant MCEE in the presence of over-expressed MUT in MCEE patient fibroblasts. Results shown represent the mean and standard deviation of 3 independent experiments.

Supplemental Fig. S6A). To determine if MUT or MCEE was rate-limiting for succinate production, we expressed each individually, or together (Fig. 5B; Supplemental Fig. S6B–C). While over-expressed MUT-alone only marginally increased detectable [^{14}C]-succinic acid, MCEE expression alone, and especially co-expression with MUT, provided a marked increase in [^{14}C]-succinic acid (Fig. 5B; Supplemental Fig. 6D). Therefore, MCEE appears to be the rate-limiting step in this pathway. This same basic pattern could be seen in MCEE null fibroblasts (Fig. 5C).

We further examined the effect of the mutant MCEE proteins in the presence of over-expressed MUT in MCEE null fibroblast lysates (Fig. 5D). Over-expression of MCEE harbouring p.Ile53Arg resulted in very little detectable [^{14}C]-succinate. This is consistent with an inability to convert D-methylmalonyl-CoA to L-methylmalonyl-CoA due to a lack of correctly folded protein, as was demonstrated by Western blot analysis. By contrast, over-expressed MCEE harbouring p.Lys60Gln produced similar levels of detectable succinate as wt protein. Finally, despite being well expressed, MCEE harbouring p.Arg143Cys had markedly reduced [^{14}C]-succinic acid production, agreeing with the significantly altered local environment in the $hMCEE_{R143C}$ structure. This conformational change could impair enzymatic activity of p.Arg143Cys either by direct structural interference with the active site, or indirectly e.g. via loss of essential interactions with other proteins in the succinyl-CoA production pathway.

4. Conclusions

The identification of an additional ten patients with MCEE deficiency adds more information toward the debate of whether deficiency of this protein does indeed cause disease and not just elevated methylmalonic acid levels. It also confirms that complete MCEE deficiency, despite incomplete penetrance, may be associated with an acute clinical phenotype with metabolic crisis resembling classical organic acidurias. However, in comparison to the most frequent organic acidurias (e.g. complete methylmalonyl-CoA deficiency, propionic acidemia), MCEE deficiency is clearly clinically less severe [24]. Our combined structural, biophysical and enzymatic assessment of MCEE defects confirm the importance of this protein within the propionate degradation pathway. While protein-destabilizing variations (e.g. p.Ile53Arg) explains enzymatic defects more readily, those away from the active-site (e.g. p.Arg143Cys) could still cause a loss of activity, although the underlying mechanism needs further clarification. With regard to p.Lys60Gln, however, we could identify no defect conferred to the protein. While we cannot rule out potential effects on mRNA splicing or protein-protein interactions, the molecular mechanism of disease caused by this variation remains unexplained.

Author contributions

D.S.F., B.F., M.R.B. and W.W.Y. conceived of the project. D.S.F., P.B. and W.W.Y. designed the research. P.B., D.S.F. and W.W.Y. analysed the results. D.S.F. performed the size exclusion chromatography. K.H. performed the Western blots and [^{14}C]-propionyl-CoA enzymatic assay. H.J.B. performed biophysical characterization of MCEE variants. C.B. sequenced the patients and identified the variations. S.L. and T.S. performed the propionic acid incorporation assay. D.S.F., E.K. and H.J.B. produced the recombinant proteins. A.C. and H.J.B. solved the crystal structures. D.S.F. and W.W.Y. wrote the paper with contributions from other authors.

Transparency document

The Transparency document associated with this article can be found, in online version.

Acknowledgements

This work was supported by the Rare Disease Initiative Zurich, a Clinical Research Priority Program from the University of Zurich (to D. S. F. and M. R. B.) and the Swiss National Science Foundation [SNSF 31003A_175779] (to M.R.B.). The SGC is a registered charity (number 1097737) that receives funds from AbbVie, Bayer Pharma AG, Boehringer Ingelheim, Canada Foundation for Innovation, Eshelman Institute for Innovation, Genome Canada, Innovative Medicines Initiative (EU/EFPIA) [ULTRA-DD grant no. 115766], Janssen, MSD, Merck KGaA, Novartis Pharma AG, Ontario Ministry of Economic Development and Innovation, Pfizer, São Paulo Research Foundation-FAPESP, Takeda and Wellcome Trust [106169/ZZ14/Z]. We thank Dr. Holger Blessing (Universitätsklinikum Erlangen, Germany), Dr. Ernst Christensen (Rigshospitalet, Copenhagen, Denmark), Dr. Andrew Morris (Alder Hey, Liverpool, UK), Dr. Murray Bain (St. George's Hospital Medical School, London, UK), Dr. Mike Champion (St. Thomas' Hospital, London, UK), Dr. W.C.G. Overweg-Plandsoen (Academisch Ziekenhuis bij de Universiteit van Amsterdam, Netherlands), Dr. Dorothea Möslinger (Universitätsklinik für Kinder und Jugendliche, Wien, Austria), Dr. Anne-Margret Wingen (Universitätsklinikum Essen, Germany) and Dr. Ina Knerr (University Children's Hospital, Dublin, Ireland) for sending patient material and data. We thank the Diamond Light Source for access to the beamlines and Carmen Diez-Fernandez for critical comments on the manuscript.

Appendix A. Supplementary data

Supplementary data to this article can be found online at https://doi.org/10.1016/j.bbadis.2019.01.021.

References

[1] C.M. Dobson, A. Gradinger, N. Longo, X. Wu, D. Leclerc, J. Lerner-Ellis, M. Lemieux, C. Belair, D. Watkins, D.S. Rosenblatt, R.A. Gravel, Homozygous nonsense mutation in the MCEE gene and siRNA suppression of methylmalonyl-CoA epimerase expression: a novel cause of mild methylmalonic aciduria, Mol. Genet. Metab. 88 (2006) 327–333.
[2] H. Bikker, H.D. Bakker, N.G. Abeling, B.T. Poll-The, W.J. Kleijer, D.S. Rosenblatt, H.R. Waterham, R.J. Wanders, M. Duran, A homozygous nonsense mutation in the methylmalonyl-CoA epimerase gene (MCEE) results in mild methylmalonic aciduria, Hum. Mutat. 27 (2006) 640–643.
[3] A.B. Gradinger, C. Belair, L.C. Worgan, C.D. Li, J. Lavallee, D. Roquis, D. Watkins, D.S. Rosenblatt, Atypical methylmalonic aciduria: frequency of mutations in the methylmalonyl CoA epimerase gene (MCEE), Hum. Mutat. 28 (2007) 1045.
[4] M. Mazzuca, M.A. Maubert, L. Damaj, F. Clot, M. Cadoudal, C. Dubourg, S. Odent, J.F. Benoit, N. Bahi-Buisson, L. Christa, P. de Lonlay, Combined sepiapterin reductase and methylmalonyl-CoA epimerase deficiency in a second patient: cerebrospinal fluid polyunsaturated fatty acid level and follow-up under L-DOPA, 5-HTP and BH4 trials, JIMD Rep. 22 (2015) 47–55.
[5] P.J. Waters, F. Thuriot, J.T. Clarke, S. Gravel, D. Watkins, D.S. Rosenblatt, S. Levesque, Methylmalonyl-coA epimerase deficiency: a new case, with an acute metabolic presentation and an intronic splicing mutation in the MCEE gene, Mol. Genet. Metab. Rep. 9 (2016) 19–24.
[6] L. Abily-Donval, S. Torre, A. Samson, B. Sudrie-Arnaud, C. Acquaviva, A.M. Guerrot, J.F. Benoist, S. Marret, S. Bekri, A. Tebani, Methylmalonyl-CoA epimerase deficiency mimicking propionic aciduria, Int. J. Mol. Sci. 18 (2017).
[7] R.N. Armstrong, Mechanistic diversity in a metalloenzyme superfamily, Biochemistry 39 (2000) 13625–13632.
[8] P. He, G.R. Moran, Structural and mechanistic comparisons of the metal-binding members of the vicinal oxygen chelate (VOC) superfamily, J. Inorg. Biochem. 105 (2011) 1259–1272.
[9] E.C. Meng, P.C. Babbitt, Topological variation in the evolution of new reactions in functionally diverse enzyme superfamilies, Curr. Opin. Struct. Biol. 21 (2011) 391–397.
[10] A.A. McCarthy, H.M. Baker, S.C. Shewry, M.L. Patchett, E.N. Baker, Crystal structure of methylmalonyl-coenzyme A epimerase from P. shermanii: a novel enzymatic function on an ancient metal binding scaffold, Structure 9 (2001) 637–646.
[11] L. Shi, P. Gao, X.X. Yan, D.C. Liang, Crystal structure of a putative methylmalonyl-coenzyme A epimerase from thermoanaerobacter tengcongensis at 2.0 A resolution, Proteins 77 (2009) 994–999.
[12] R.B. Hamed, J.R. Gomez-Castellanos, D. Sean Froese, E. Krysztofinska, W.W. Yue, C.J. Schofield, Use of methylmalonyl-CoA epimerase in enhancing crotonase stereoselectivity, Chembiochem 17 (2016) 471–473.
[13] A. Chaikuad, S. Knapp, F. von Delft, Defined PEG smears as an alternative approach

to enhance the search for crystallization conditions and crystal-quality improvement in reduced screens, Acta Crystallogr. D Biol. Crystallogr. 71 (2015) 1627–1639.
[14] A.J. McCoy, Solving structures of protein complexes by molecular replacement with Phaser, Acta Crystallogr. D Biol. Crystallogr. 63 (2007) 32–41.
[15] P. Emsley, B. Lohkamp, W.G. Scott, K. Cowtan, Features and development of Coot, Acta Crystallogr. D Biol. Crystallogr. 66 (2010) 486–501.
[16] G.N. Murshudov, A.A. Vagin, E.J. Dodson, Refinement of macromolecular structures by the maximum-likelihood method, Acta Crystallogr. D Biol. Crystallogr. 53 (1997) 240–255.
[17] P.D. Adams, P.V. Afonine, G. Bunkoczi, V.B. Chen, I.W. Davis, N. Echols, J.J. Headd, L.W. Hung, G.J. Kapral, R.W. Grosse-Kunstleve, A.J. McCoy, N.W. Moriarty, R. Oeffner, R.J. Read, D.C. Richardson, J.S. Richardson, T.C. Terwilliger, P.H. Zwart, PHENIX: a comprehensive python-based system for macromolecular structure solution, Acta Crystallogr. D Biol. Crystallogr. 66 (2010) 213–221.
[18] T. Plessl, C. Burer, S. Lutz, W.W. Yue, M.R. Baumgartner, D.S. Froese, Protein destabilization and loss of protein-protein interaction are fundamental mechanisms in cblA-type methylmalonic aciduria, Hum. Mutat. 38 (2017) 988–1001.
[19] M. Lek, K.J. Karczewski, E.V. Minikel, K.E. Samocha, E. Banks, T. Fennell, A.H. O'Donnell-Luria, J.S. Ware, A.J. Hill, B.B. Cummings, T. Tukiainen, D.P. Birnbaum, J.A. Kosmicki, L.E. Duncan, K. Estrada, F. Zhao, J. Zou, E. Pierce-Hoffman, J. Berghout, D.N. Cooper, N. Deflaux, M. DePristo, R. Do, J. Flannick, M. Fromer, L. Gauthier, J. Goldstein, N. Gupta, D. Howrigan, A. Kiezun, M.I. Kurki, A.L. Moonshine, P. Natarajan, L. Orozco, G.M. Peloso, R. Poplin, M.A. Rivas, V. Ruano-Rubio, S.A. Rose, D.M. Ruderfer, K. Shakir, P.D. Stenson, C. Stevens, B.P. Thomas, G. Tiao, M.T. Tusie-Luna, B. Weisburd, H.H. Won, D. Yu, D.M. Altshuler, D. Ardissino, M. Boehnke, J. Danesh, S. Donnelly, R. Elosua, J.C. Florez, S.B. Gabriel, G. Getz, S.J. Glatt, C.M. Hultman, S. Kathiresan, M. Laakso, S. McCarroll, M.I. McCarthy, D. McGovern, R. McPherson, B.M. Neale, A. Palotie, S.M. Purcell, D. Saleheen, J.M. Scharf, P. Sklar, P.F. Sullivan, J. Tuomilehto, M.T. Tsuang, H.C. Watkins, J.G. Wilson, M.J. Daly, D.G. MacArthur, C. Exome Aggregation, Analysis of protein-coding genetic variation in 60,706 humans, Nature 536 (2016) 285–291.
[20] P. Forny, D.S. Froese, T. Suormala, W.W. Yue, M.R. Baumgartner, Functional characterization and categorization of missense mutations that cause methylmalonyl-CoA mutase (MUT) deficiency, Hum. Mutat. 35 (2014) 1449–1458.
[21] M.R. Baumgartner, S. Almashanu, T. Suormala, C. Obie, R.N. Cole, S. Packman, E.R. Baumgartner, D. Valle, The molecular basis of human 3-methylcrotonyl-CoA carboxylase deficiency, J. Clin. Invest. 107 (2001) 495–504.
[22] T. Suormala, M.R. Baumgartner, D. Coelho, P. Zavadakova, V. Kozich, H.G. Koch, M. Berghauser, J.E. Wraith, A. Burlina, A. Sewell, J. Herwig, B. Fowler, The cblD defect causes either isolated or combined deficiency of methylcobalamin and adenosylcobalamin synthesis, J. Biol. Chem. 279 (2004) 42742–42749.
[23] J. Schymkowitz, J. Borg, F. Stricher, R. Nys, F. Rousseau, L. Serrano, The FoldX web server: an online force field, Nucleic Acids Res. 33 (2005) W382–W388.
[24] S.C. Grunert, M. Stucki, R.J. Morscher, T. Suormala, C. Burer, P. Burda, E. Christensen, C. Ficicioglu, J. Herwig, S. Kolker, D. Moslinger, E. Pasquini, R. Santer, K.O. Schwab, B. Wilcken, B. Fowler, W.W. Yue, M.R. Baumgartner, 3-methylcrotonyl-CoA carboxylase deficiency: clinical, biochemical, enzymatic and molecular studies in 88 individuals, Orphanet J. Rare Dis. 7 (2012) 31.